CrossMark

ORIGINAL

Different arrangements of simplified models to predict effective thermal conductivity of open-cell foams

Prashant Kumar[1] · Frédéric Topin[1]

Abstract It is often desirable to predict the effective thermal conductivity (ETC) of a homogenous material like open-cell foams based on its composition, particularly when variations in composition are expected. A combination of five fundamental simplified thermal conductivity bounds and models (series, parallel, Hashin–Shtrikman, effective medium theory, and reciprocity models) is proposed to predict ETC of open-cell foams. Usually, these models use a parameter as the weighted mean to account the proportion of each bound arranged in arithmetic and geometric schemes. Based on ETC data obtained on numerous virtual Kelvin-like foam samples, the dependence of this parameter has been deduced as a function of morphology and phase thermal conductivity ratio. Various effective thermal conductivity correlations are derived based on material properties and foam structure. This is valid for open-cell foams filled with any arbitrary working fluid over a solid conductivity of materials range ($\lambda_s/\lambda_f = 10$–30,000) and over a wide range of porosity ($0.60 < \varepsilon_o < 0.95$). Arrangement of series and parallel models together using the simplest models for both, arithmetic and geometric schemes, is found to predict excellent results among all the generic combinations.

Abbreviations

μCT	Micro-computed tomography
ETC	Effective thermal conductivity
EMT	Effective medium theory
HS	Hashin–Shtrikman
LBM	Lattice Boltzmann method
RT	Reciprocity theorem

List of symbols

Latin symbols

A or R	Side length of strut shape or radius of strut shape (mm)
L_c	Node-to-node length (mm)
L_s	Strut length (mm)
F	Correlation factor (Eq. 30)
R_{eq}	Equivalent circular strut radius (mm)

Greek symbols

ε_o	Open porosity
ε_t	Total porosity
α_{eq}	Ratio of equivalent circular strut radius to node-to-node length
β	Ratio of strut length to node-to-node length
δ	Functional parameter in arithmetic scheme (Eq. 7)
δ'	Functional parameter in geometric scheme (Eq. 8)
ψ	Dimensionless geometrical parameter (Eq. 23)
η	Dimensionless fitting parameter (Eqs. 27 and 29)
η'	Dimensionless fitting parameter (Eq. 28)
λ_s	Intrinsic solid phase conductivity of foam (W m^{-1} K^{-1})
λ_s^B	Solid/Bulk phase conductivity of foam material (W m^{-1} K^{-1})
λ_f	Fluid phase conductivity (W m^{-1} K^{-1})
λ_{eff}	Effective thermal conductivity (W m^{-1} K^{-1})

✉ Prashant Kumar
prashant.kumar@univ-amu.fr

Frédéric Topin
frederic.topin@univ-amu.fr

[1] IUSTI, CNRS UMR 7343, Aix-Marseille Université, Marseille, France

$\lambda_{parallel}$ Effective parallel thermal conductivity (Eq. 1) (W m^{-1} K^{-1})

λ_{series} Effective series thermal conductivity (Eq. 2) (W m^{-1} K^{-1})

$\lambda_{HS,Upper}$ HS upper bound thermal conductivity (Eq. 3) (W m^{-1} K^{-1})

$\lambda_{HS,Lower}$ HS lower bound thermal conductivity (Eq. 4) (W m^{-1} K^{-1})

λ_{EMT} Effective medium theory thermal conductivity (Eq. 5) (W m^{-1} K^{-1})

λ_{RM} Reciprocity model (Eq. 6) (W m^{-1} K^{-1})

1 Introduction

The thermal conductivity of porous materials, more particularly open-cell foams, plays an important role in many industrial processes. Heat conduction takes place through a solid skeleton and a fluid passing through the 3-D interconnected network of open-cells. In order to effectively utilize open-cell foams in heat transfer applications e.g. heat exchangers, volumetric solar receiver etc., accurate knowledge of their thermal transport properties are needed.

Many heat transfer mechanisms at pore scale could be included in equivalent thermal conductivity. The effective thermal conductivity refers to the case when only diffusion plays a role. The energy transport is then controlled by the effective thermal conductivity (e.g. [1–5]). However, at high temperatures or for foam materials of extremely low conductivity, an equivalent thermal conductivity depends also on radiative heat transfer (e.g. [6–8]) for which the expression or formulation is completely different.

The ETC of open-cell foams is not only dependent on the constituent phase properties and porosity, but also on the structure of the materials (e.g. [4, 9–12]). Moreover, the intrinsic solid phase conductivity may be different from the parent/bulk material conductivity. Miettinen et al. [9] showed experimentally that there exists no simple relationship between intrinsic solid phase heat conductivity and porosity. Dietrich et al. [4] measured the thermal conductivity of strut materials and obtained a decrease in their intrinsic solid phase conductivity compared to the conductivity of pure/bulk material. Kumar et al. [10] showed a decrease of approximately 20–25% in the solid phase thermal conductivity of bulk material when transformed in foams (see also [11, 12]) from their calculated ETC data.

Apart from experiments, substantial efforts have been made in the recent years to estimate the effective thermal conductivity based on: (1) numerical simulations using X-ray μCT images of actual foam samples (e.g. [13–20]) (2) numerical simulations on idealized representation of open-cell foams (e.g. [10, 11, 21, 22]) and, (3) empirical correlations by fitting experimental data (e.g. [1, 2, 4, 5, 12, 23, 24]).

Despite accuracy and precision of ETC results obtained from numerical simulations (or experiments), they are considerably time and resource consuming. Moreover, ETC of a specific structure for a given working fluid has to be obtained individually on a case to case basis. Thus, an empirical correlation is a reasonable compromise between measurements and computational time for quick and accurate evaluation of ETC. It presents general applicability for a wide range of materials, porosities, and ratios of solid and fluid phase conductivities.

Various simplified bounds and models exist in literature to predict the ETC values for different porous media. The most common inputs for these models are material properties (e.g. solid and fluid conductivities) and material morphology (e.g. porosity). Nevertheless, prediction of ETC values for different class of materials i.e. foam like structures is not straightforward. Consequently, various authors proposed empirical correlations using these bounds/models or combination between them to predict reasonable ETC values with or without an adjustable parameter depending on the ratio of constituent phases.

In open-cell foams, the empirical value of adjustable parameter in ETC correlations varies between employed models and used type of materials. Variations in adjustable parameter are due to the preferred choice of model/bound by authors and depend usually on the type of foam material used (metallic or ceramic) and thus, resulting in a massive gap to have access to complete range of conductivity ratios. Consequently, there is no simple model that can be used for all existing types of open-cell foams.

In this work, our intent is to develop generalized ETC correlations in accessible porosity range ($0.60 < \varepsilon_o < 0.98$) of foams resembling Kelvin-like cell structure and extend the conductivity ratios range ($\lambda_s/\lambda_f = 10$–$30{,}000$) in order to fill this gap. It is from this view point, five basic arrangements of simplified models and their combinations including the series and parallel models [25], Hashin–Shtrikman upper and lower bounds [26], effective medium theory (EMT) [27], and, reciprocity model [28] are adapted as generic minimum and maximum bounds of thermal conductivity in both arithmetic and geometric schemes. A functional parameter is obtained by fitting ETC data obtained numerically from our previous works [10, 11]. Obviously, this parameter cannot be obtained beforehand but it has been determined in our present work for the whole range of porosities and thermal conductivity ratios. Thus, it could be used as a function of the traditional input parameters (foam morphology and material property: conductivities) in order to predict ETC value for any Kelvin-like foam structure.

2 Literature study of ETC correlations

We discuss here ETC as an intrinsic property of conductive heat transfer and not an apparent property representing many other unspecified heat transfer phenomena (e.g. radiation, micro-convection, dispersion, evaporation–condensation etc.). Mixing heat transfer mode in a single apparent coefficient leads to a confusing situation and prohibit comparison and use of obtained data. Nevertheless in several cases, the diffusive heat transfer is not the principal one for a given situation. This contribution could be calculated separately and added eventually (e.g. [6]).

Usually, commercially available real foams are close to periodic in nature. Pieper and Klein [29] demonstrated that the periodic homogenization for real structures close to periodic gives very accurate results. This led researchers to derive empirical correlations for quick estimation of ETC values that are generally based either on asymptotic approaches or on a micro-structural approach in case of open-cell foams. It is widely known that the ETC strongly depends on porosity and the ratio of thermal conductivities of the constituent phases but also on a lesser extent to the distributions of the solid phase (e.g. between struts and lumps) that depends on the manufacturing process. Using analytical modelling, some authors (e.g. [1, 2, 5, 14, 23, 30]) have considered lumps at the node junctions while others (e.g. [4, 10–12, 24]) did not assume the presence of lumps of matter at the node junctions while deriving their empirical correlations. Majority of these works concerns very high conductive metal foams (e.g. [1, 2, 5, 24]) in high porosity range ($0.88 < \varepsilon_o < 0.97$). On the other hand, a few works are dedicated to low conductive ceramic foams (e.g. [4]) for moderate porosity range ($0.75 < \varepsilon_o < 0.97$).

For the validation of empirical correlations against ETC data, it is henceforth of major importance to measure the intrinsic solid phase thermal conductivity of the foam sample because different commercially available foams employ different manufacturing techniques; that lead to significant changes in the intrinsic solid phase thermal conductivity of foams, compared to the same parent/bulk material [4, 9–11]. The correlations reported in the literature can be classified into three major groups that use mainly the same preferences of building correlations. Most commonly, one or two adjustable parameters that contain information about morphology are obtained by fitting experimental or numerical ETC data to derive correlations.

The first group of authors used only porosity and derived correlations based on series and bounds arranged in either geometric (e.g. [24]) or arithmetic (e.g. [4]) scheme. Note that these models do not introduce additional morphological parameters to describe ETC; although this influence has already been shown to be significant (see [10–12, 17, 18]).

The second group of authors tried to introduce other morphological parameters in their correlation based on 2-D (e.g. [1, 2]) or 3-D foam geometry (e.g. [1, 2, 5, 12, 23, 29–31]) and deduced an adjustable parameter from experimental data. Most of these correlations are limited to very high conductive materials (e.g. Al, Cu) while neglecting the influence of low conductive fluid such as air or water ($\lambda_s^B/\lambda_f > 400$). These correlations give poor estimates of ETC values for foams of different materials. Constant and variable values of adjustable parameters were obtained by fitting experimental data as a function of morphology and conductivity ratios. Contrary to this, Qu et al. [30] described a so-called 'morphological parameter' that was obtained by fitting the experimental ETC data is rather material dependent (thermal conductivity ratio) instead of foam morphology and is only valid for a few types of foam materials. Kumar and Topin [12] derived ETC correlation for low conductive ceramic foam materials ($150 < \lambda_s/\lambda_f < 900$) and modified the Lemlich approach. Their models could be used together to predict the intrinsic solid phase conductivity of foams of different materials irrespective of fluid phase and porosity when ETC is known.

The third of group of authors calculated ETC from numerical solution of heat equation on idealized or reconstructed open and closed foam structures (e.g. [7, 10–20, 22]). Pore scale numerical simulations (using finite element, finite volume and Lattice-Boltzmann methods) allow solving heat equation within both solid and fluid phases on such foam structures while varying porosity, morphology and conductivity ratios. Druma et al. [22] concluded that some simplified models could not accurately predict the ETC of foams (approximated by spherical pores, homogeneously dispersed within a solid matrix) over the complete range of porosities. Coquard and Baillis [14] deduced that the realistic representations of foam structures (e.g. Cubic, Tetrakaidecahedron and Weaire-Phelan unit cells) did not account for the commercial foam irregularities and imperfections. Mendes et al. [17] observed that using HS bounds to build an ETC correlation give the best results for most of the investigated foam structures. They also proposed an empirical correlation using a complex arrangement of Series and Parallel models [18]. In both cases, the adjustable parameters can only be obtained from the complete set of ETC data. Kumar et al. [10] performed numerical simulations on Kelvin-like cell structure with convex triangular cross section ligaments to determine ETC over a wide range of solid to fluid conductivity ratios. The weighted factor appearing in their correlation is deduced from the morphological parameters and the ratio of solid to fluid phase thermal conductivities. This work was further extended to different strut

cross-sections [11]. These authors found that the cell size and the strut cross section shape have negligible effects on ETC.

3 Simplified ETC models of porous media

The effective thermal conductivity of open-cell foams is much higher than those of the granular porous media. Since the solid has a higher conductivity, the interconnected microstructure virtually increases the pathway of thermal conduction (or energy flux) in the homogenous medium compared with the discrete granular microstructure, and therefore enhances the effective thermal conductivity of the foam material.

Two models of a two-phase material, which are not themselves realistic for a foam but provide useful results are the "parallel" and "series" models illustrated in Fig. 1a, b, respectively and are often used as benchmarks for new model validations. The physical structures assumed in the derivations of the Series and Parallel models are layers of the components aligned either perpendicular or parallel to the heat flux as presented in Eqs. 1 and 2.
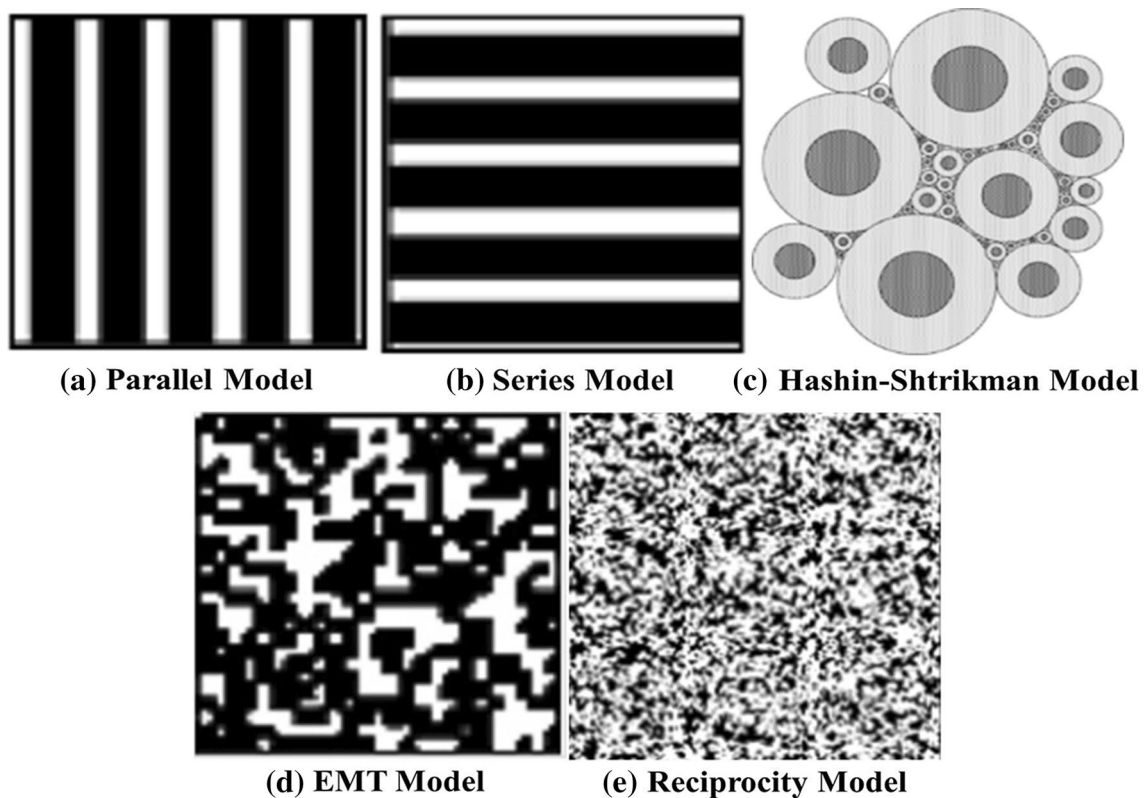
$$\lambda_{parallel} = (1 - \varepsilon_o)\lambda_s + \varepsilon_o\lambda_f \tag{1}$$

$$\lambda_{series} = \frac{\lambda_s \cdot \lambda_f}{(1 - \varepsilon_o)\lambda_f + \varepsilon_o\lambda_s} \tag{2}$$

Hashin and Shtrikman [26] derived effective conductivity bounds on the basis of a variational approach that were the best (i.e. narrowest) possible bounds for macroscopically homogeneous, isotropic, two-phase materials that could be derived from the components' volume fractions and conductivities. The bounds state that the ETC of any isotropic mixture of several isotropic conducting materials satisfies certain inequalities independently of the structure of a porous medium (see Fig. 1c). The Hashin–Shtrikman (HS) bounds always lie within the Series–Parallel bounds, regardless of the components volume fractions or thermal conductivities and are given by Eqs. 3 and 4.

$$\lambda_{HS,Upper} = \lambda_s\left[\frac{2\lambda_s + \lambda_f - 2(\lambda_s - \lambda_f)\varepsilon_o}{2\lambda_s + \lambda_f + (\lambda_s - \lambda_f)\varepsilon_o}\right] \tag{3}$$

$$\lambda_{HS,Lower} = \lambda_f\left[\frac{2\lambda_f + \lambda_s - 2(\lambda_f - \lambda_s)(1 - \varepsilon_o)}{2\lambda_f + \lambda_s + (\lambda_f - \lambda_s)(1 - \varepsilon_o)}\right] \tag{4}$$

(a) Parallel Model   **(b) Series Model**   **(c) Hashin-Shtrikman Model**

(d) EMT Model   **(e) Reciprocity Model**

Fig. 1 Five fundamental effective thermal conductivity structural models for two-component (solid and fluid phases) open-cell foam materials (assuming the heat flow is in the vertical direction)

The problem of electrical conduction in an inhomogeneous medium could be solved by the effective medium theory (EMT). Laudauer's EMT model [27] consists of a two-component medium composed of two different materials, with neither phase being necessarily continuous or dispersed. The shape of each material element is assumed to be spherical. The main assumption in Landauer's theory is that the medium surrounding an element is considered homogenous, which has an effective conductivity that characterizes the overall properties of the mixture (see Fig. 1d). Either component may form continuous heat conduction pathways, depending on the relative amounts of the components, making this structure unbiased towards its components. Moreover, for porous media in which the solid phase forms continuous pathways, such as open-cell foams, the minimum ETC bound is expected to be given by the effective medium theory (EMT) as given in Eq. 5.

$$\lambda_{EMT} = \frac{1}{4}\Big[(3\varepsilon_o - 1)\lambda_f + \{3(1-\varepsilon_o) - 1\}\lambda_s$$
$$+ \sqrt{\left[(3\varepsilon_o - 1)\lambda_f + \{3(1-\varepsilon_o) - 1\}\lambda_s\right]^2 + 8\lambda_f\lambda_s}\Big]$$

$$(5)$$

The reciprocity model was based on the reciprocity theorem [28] which assumes that a microstructure of two-component remains statistically equivalent when exchanging the volume fractions of the components (see Fig. 1e) and is given by Eq. 6. Reciprocity model is quite different than other models and predictions agreed well with many granular materials of spherical nature [32].

$$\frac{\lambda_{RM}}{\lambda_f} = \frac{1 + \left(\sqrt{\lambda_f/\lambda_s} - 1\right)\varepsilon_o}{1 + \left(\sqrt{\lambda_s/\lambda_f} - 1\right)\varepsilon_o} \tag{6}$$

4 Comparison between experimental and numerical ETC

Most of the ETC data were reported in the literature for the cases where λ_s (or λ_s^B) $\gg \lambda_f$ (usually metal foams). In order to perform numerical simulations to calculate ETC of foam samples, it is necessary to provide solid and fluid conductivities as an input parameters on foam structures. As discussed in Sects. 1 and 2, intrinsic solid phase thermal conductivity of foam materials (λ_s) has not been generally measured in majority of the works. It is from this view point, we chose to perform numerical simulations using the measured intrinsic solid phase conductivities of Al_2O_3, Mullite and OBSiC ceramic foams (λ_s = 26, 4.4, 15 W m^{-1} K^{-1} respectively) by Dietrich et al. [4]. The fluid conductivity (λ_f) of air used was 0.03 W m^{-1} K^{-1}.

As ETC is mainly porosity driven, virtual open-cell foams were generated based on total porosity (ε_t) reported by Dietrich et al. [4]. 3-D numerical simulations at pore scale were performed on these virtual open-cell foams with circular strut cross-section in LTE condition (for detailed description, see our previous work [11]). In the Fig. 2, total porosity as well as ETC data obtained numerically were compared against experimental data and are in excellent agreement. However, there are very minimal differences which could be attributed to the measurements uncertainties, numerical errors and morphological disparity. This agreement confirms quantitatively and qualitatively the previously published numerical dataset of ETC, which lends confidence to develop different ETC configurations based on different simplified models.
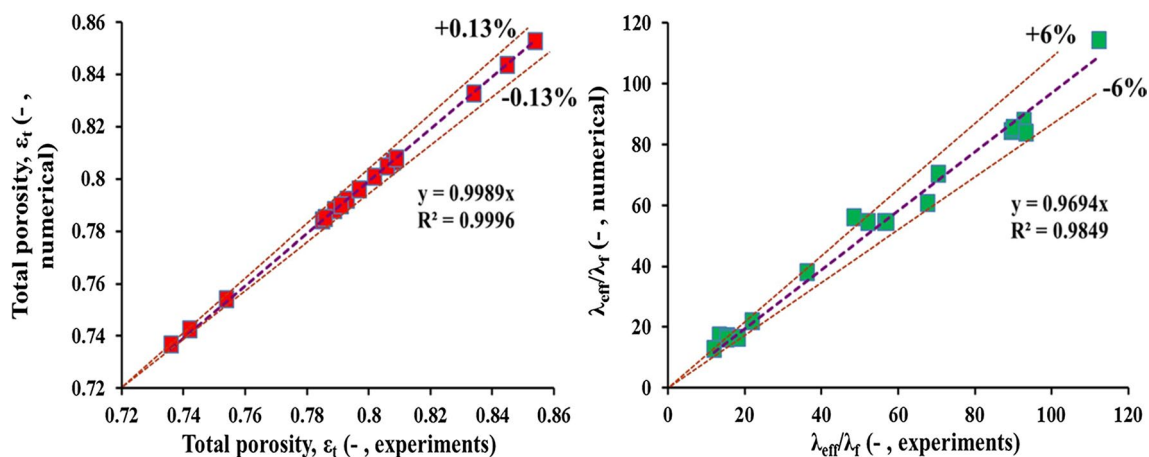
Fig. 2 Comparison and validation of experimental ETC data (taken from the works of Dietrich et al. [4]) against numerically calculated ETC data of ceramic foams

5 Empirical modelling of effective thermal conductivity

Depending on the availability of foam material (ceramic, alloys and pure metals), authors found out different values of adjustable parameters based on different arrangement of bounds. These adjustable parameters possessed fixed (e.g. [4, 23, 31]) and variable (e.g. [10–12, 24]) values in the most of the reported works. On the other hand, a few authors did not obtain any adjustable parameter in ETC determination for very high conductive material. The most common belief in this case is that heat conduction is mainly due to solid conductivity occurring mainly through the parallel layout while neglecting the influence of working fluid conductivity like air or water.

The present work investigates in predicting ETC values by determining a functional parameter in terms of the traditional input parameters valid for the complete range of porosities and accessible thermal conductivity ratios of Kelvin-like foams. This has been carried out by arranging various combinations of simplified bounds and models (see Eqs. 7 and 8).

As a first step, a generalization of the simplified model for ETC similar to the works of Mendes et al. [17] is proposed in the arithmetic scheme as presented in Eq. 7. This approach is extended and applied to a geometric scheme (also proposed by a few authors e.g. [10–12, 24]) as described in Eq. 8. The two schemes are chosen in order to identify how simple models can be best arranged based on generic minimum and maximum bounds and could predict accurate ETC values of open-cell foams.

$$\lambda_{eff} = \delta\lambda_{min} + (1 - \delta)\lambda_{max} \tag{7}$$

$$\lambda_{eff} = \lambda_{max}^{\delta'} \cdot \lambda_{min}^{1-\delta'} \tag{8}$$

where, λ_{max} and λ_{min} are generic maximum and minimum bounds for the ETC respectively, and δ and δ' are the functional parameters to be determined from the fitting of various experimental/numerical data.

Mendes et al. [17] used an adjustable parameter δ that was an explicit function of the structure of porous media and obtained by calculating ETC of solid phase alone (i.e. under vacuum condition). δ values were obtained for each case from numerical simulations by giving $\lambda_{eff,s}$ and respective values for λ_{min} and λ_{max} under vacuum conditions.

A different strategy is applied in the current work to obtain the parameters, δ and δ' by solving Eqs. 7 and 8 in terms of λ_{eff}, λ_{min} and λ_{max} as:

$$\delta = \frac{\lambda_{max} - \lambda_{eff}}{\lambda_{max} - \lambda_{min}} \tag{9}$$

$$\delta' = \frac{ln(\lambda_{eff}) - ln(\lambda_{min})}{ln(\lambda_{max}) - ln(\lambda_{min})} \tag{10}$$

where, $0 < \delta \,(\text{or } \delta') < 1$.

Based on the proposed generic ETC model, given by Eqs. 9 and 10, and considering different possible minimum ($\lambda_{min} = \lambda_{series}, \lambda_{HS,Lower}, \lambda_{EMT}$ and λ_{RM}) and maximum ($\lambda_{max} = \lambda_{parallel}$ and $\lambda_{HS,Upper}$) bounds, twelve different arrangements of these models are formed (Models 1–12, six for each scheme, Eqs. 11–22 in Table 1) by selecting different expressions for λ_{max} and λ_{min}. In the following sections, they are called as "model" for the sake of simplicity.

These models are presented in Table 1 where explicit expressions of δ and δ' are provided. The dataset of 2000 numerically obtained values of ETC obtained on virtual and ideal isotropic foam structures was gathered from our previous work [11] to determine values of δ and δ' in order

Table 1 Simplified models for effective thermal conductivity, based on the generic model given by Eqs. 9 and 10, obtained by selecting different thermal arrangements for λ_{min} and λ_{max}

λ_{min}	λ_{max}	Arithmetic scheme			Geometric scheme		
		Configuration nos.	δ (using Eq. 9)	Eq. nos.	Model no.	δ' (using Eq. 10)	Eq. nos.
λ_{series}	$\lambda_{parallel}$	Model 1	$\delta_1 = \frac{\lambda_{parallel} - \lambda_{eff}}{\lambda_{parallel} - \lambda_{series}}$	11	Model 7	$\delta'_1 = \frac{ln(\lambda_{eff}) - ln(\lambda_{series})}{ln(\lambda_{parallel}) - ln(\lambda_{series})}$	17
$\lambda_{HS,Lower}$	$\lambda_{HS,Upper}$	Model 2	$\delta_2 = \frac{\lambda_{HS,Upper} - \lambda_{eff}}{\lambda_{HS,Upper} - \lambda_{HS,Lower}}$	12	Model 8	$\delta'_2 = \frac{ln(\lambda_{eff}) - ln(\lambda_{HS,Lower})}{ln(\lambda_{HS,Upper}) - ln(\lambda_{HS,Lower})}$	18
λ_{EMT}	$\lambda_{parallel}$	Model 3	$\delta_3 = \frac{\lambda_{parallel} - \lambda_{eff}}{\lambda_{parallel} - \lambda_{EMT}}$	13	Model 9	$\delta'_3 = \frac{ln(\lambda_{eff}) - ln(\lambda_{EMT})}{ln(\lambda_{parallel}) - ln(\lambda_{EMT})}$	19
λ_{EMT}	$\lambda_{HS,Upper}$	Model 4	$\delta_4 = \frac{\lambda_{HS,Upper} - \lambda_{eff}}{\lambda_{HS,Upper} - \lambda_{EMT}}$	14	Model 10	$\delta'_4 = \frac{ln(\lambda_{eff}) - ln(\lambda_{EMT})}{ln(\lambda_{HS,Upper}) - ln(\lambda_{EMT})}$	20
λ_{RM}	$\lambda_{parallel}$	Model 5	$\delta_5 = \frac{\lambda_{parallel} - \lambda_{eff}}{\lambda_{parallel} - \lambda_{RM}}$	15	Model 11	$\delta'_5 = \frac{ln(\lambda_{eff}) - ln(\lambda_{RM})}{ln(\lambda_{parallel}) - ln(\lambda_{RM})}$	21
λ_{RM}	$\lambda_{HS,Upper}$	Model 6	$\delta_6 = \frac{\lambda_{HS,Upper} - \lambda_{eff}}{\lambda_{HS,Upper} - \lambda_{RM}}$	16	Model 12	$\delta'_6 = \frac{ln(\lambda_{eff}) - ln(\lambda_{RM})}{ln(\lambda_{HS,Upper}) - ln(\lambda_{RM})}$	22

to account for a wide range of porosities, different morphological parameters of foam structures as well as low to high ratios of solid to fluid conductivity ratios. Previously, porosity (ε_o) of an idealized isotropic Kelvin-like cell was expressed as a function of dimensionless morphological parameters (ψ) of foams of any strut cross section [10–12] (Eq. 23).

Same procedure was followed and δ values for minimum and maximum bounds arranged in arithmetic scheme were plotted against ψ for Models 1–6 (see Eqs. 11–16) based on Eq. 9. It can be seen in Fig. 3a, c corresponding to the Model 1 (λ_{series} and $\lambda_{parallel}$ bounds) and Model 3 (λ_{EMT} and $\lambda_{parallel}$ bounds), δ values (obtained from Eq. 9
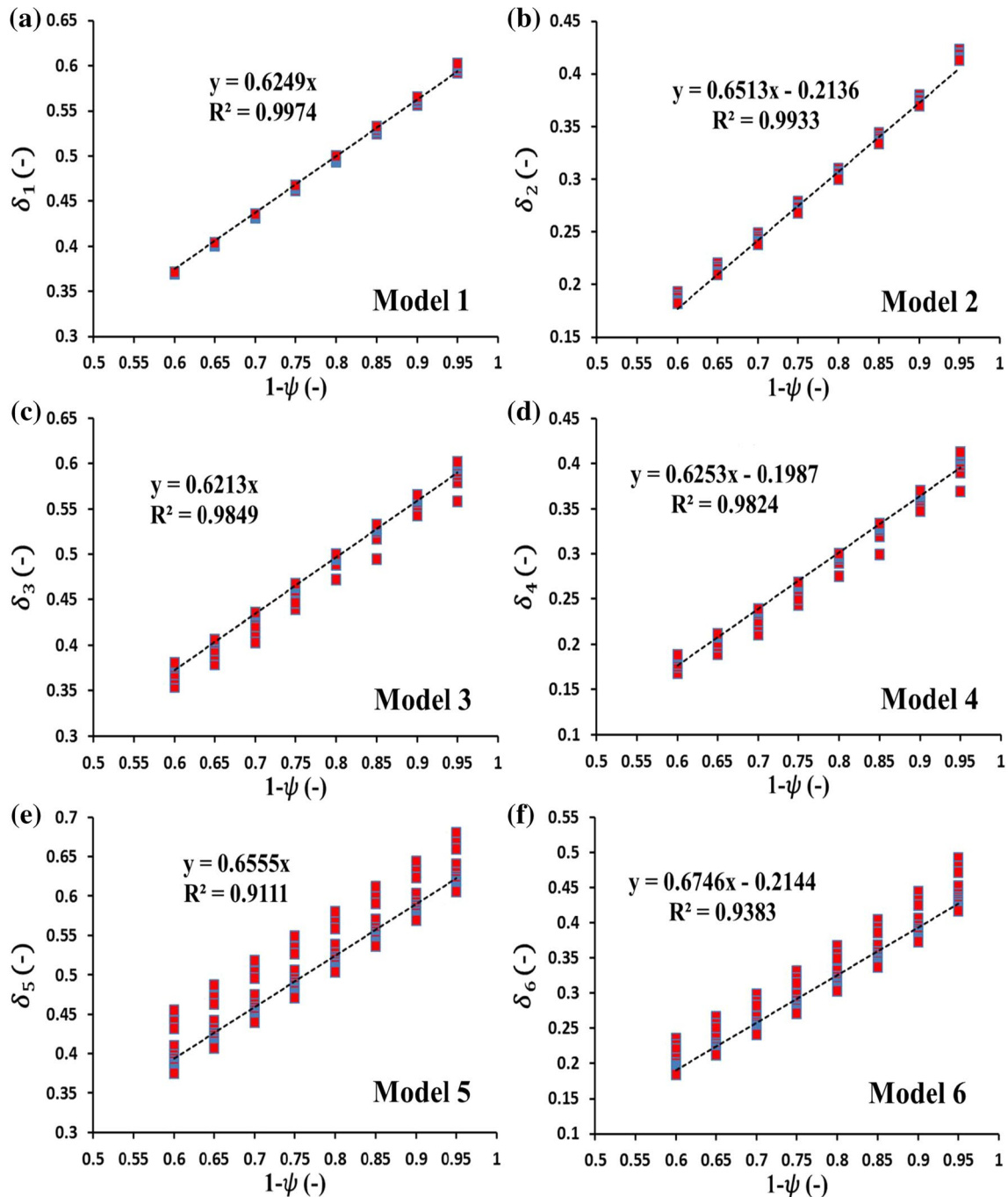
Fig. 3 Plot of δ (dimensionless) for different arrangements of simplified models (Models 1–6) in arithmetic scheme. The *dotted line* represents the best fitting of δ values calculated using Eq. 9 from numerical ETC values of Kumar and Topin [11] corresponding to different Models (1–6). *Different colours* of cubic data points represent δ values obtained for different porosities (colour figure online)

using numerical ETC values [11]) collapse very well and a unique curve is obtained as presented in Eqs. 24–25.

$$1 - \varepsilon_o = \psi = 12\pi\alpha_{eq}^2\beta + \frac{32}{3}\pi\alpha_{eq}^3 \tag{23}$$

$$\delta_1 = 0.6249(1 - \psi) \tag{24}$$

$$\delta_3 = 0.6213(1 - \psi) \tag{25}$$

where $\alpha_{eq} = R_{eq}/L_c$ (ratio of equivalent circular strut radius to node-to-node length) and $\beta = L_s/L_c$ (ratio of strut length to node-to-node length) respectively. This formulation (Eq. 23) is presented in [11].

The RMSD (root-mean-square-difference) values (see Eq. 26) are 0.77 and 1.93% for δ values of Models 1 and 3.

$$RMSD = 10^{RMS(ELOG)} - 1 \; with \; ELOG = \log(\delta)_{calc} - log(\delta)_{exp} \tag{26}$$

In case of Model 2 ($\lambda_{HS,Lower}$ and $\lambda_{HS,Upper}$ bounds), data of δ values fit very well (see Fig. 3b). An intercept has been introduced in order to obtain the best fit of ETC data. However, no explanation is yet found for the meaning of the intercept. The models 4–6 (see Fig. 3d, f) clearly indicate that they follow same trend with porosity but do not form unique characteristics. However, these fittings are not coherent over the entire range of porosity and thus, they are not suitable to be arranged in arithmetic scheme to predict accurate values of ETC.

In the case of arrangements of simplified models in geometric scheme, the derivation of an empirical correlation is more difficult to obtain an excellent combination of dimensionless morphological parameters and ratio of constituent phases. The geometric scheme of series and parallel models

using a weighted parameter (Model 7, Eq. 17) has already been presented [10–12] and thus, this scheme is not shown here. Following their procedure, δ' values for Models 8–12 (see Eqs. 18–22) are calculated (obtained from Eq. 10 using numerical ETC values [11]) and further efforts have been made to obtain an accurate relation between δ' and a combination of ψ and λ_s/λ_f as presented in Fig. 4. However, we could not advance to obtain any relationship between δ', ψ and λ_s/λ_f for Models 9 and 10. The plots of δ_2', δ_5' and δ_6' are represented against $\eta = ln(\psi^{2.25}\lambda_s/\lambda_f)$, $\eta' = ln(\psi^{1.5}\lambda_s/\lambda_f)$ and $\eta = ln(\psi^{2.25}\lambda_s/\lambda_f)$ in Fig. 4a–c respectively. The dimensionless parameters η (and η') are the best fitting parameters to estimate effective thermal conductivity (using Eq. 8). It can be easily observed that all the values of δ' in relation with η (and η') collapsed on a single curve for all the different strut shapes. The RMSD values are 1.04, 1.82 and 1.6% for Models 8, 11, and 12 respectively, obtained just by replacing δ with δ' in Eq. 26. From Fig. 4, numerical approximation of δ' for Models 8, 11, and 12 are given by Eqs. 27–29 as:

$$\delta_2' = -0.0028\eta^2 + 0.0395\eta + 0.8226 \tag{27}$$

$$\delta_5' = -0.005\eta'^2 + 0.0876\eta' + 0.4914 \tag{28}$$

$$\delta_6' = -0.0029\eta^2 + 0.0458\eta + 0.759 \tag{29}$$

There is no physical reason to choose a quadratic polynomial function in Eqs. 27–29 and we do not claim any physical meaning to the curve fitting. The quadratic polynomial function is the simplest function that gives a good approximation of ETC data.

The development of functional parameter, δ (or δ') is clearly a function of foam morphology (ψ) and constituent conductivities (λ_s/λ_f) depending the combination of
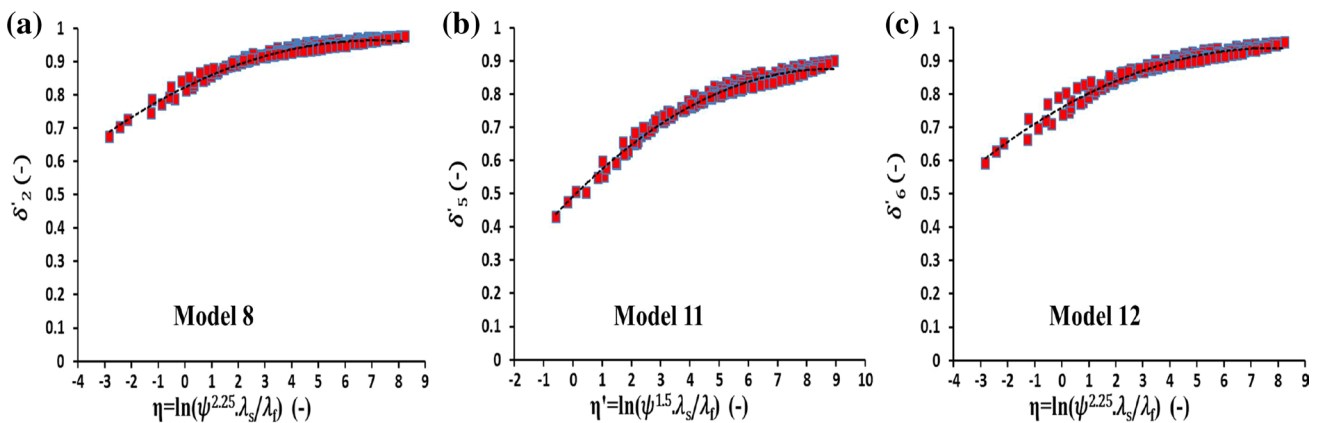
Fig. 4 Plot of δ' (dimensionless) versus fitting parameters η and η' (dimensionless) of different strut shapes. **a** Model 8–plot of δ_2' versus $\eta = ln(\psi^{2.25}\lambda_s/\lambda_f)$. **b** Model 11—plot of δ_5' versus $\eta' = ln(\psi^{1.5}\lambda_s/\lambda_f)$. **c** Model 12—plot of δ_6' versus $\eta = ln(\psi^{2.25}\lambda_s/\lambda_f)$. The errors in these models are evenly distributed. *Different colours* of cubic data points represent δ' values obtained for different porosities (colour figure online)

bounds and models employed. For each combination, the functional parameter is unique. Figure 5 presents a simple algorithm to predict ETC from input parameters for foam structures. Moreover, this algorithm can also be used to predict the solid phase conductivity and morphology from a known ETC value that could help in optimizing foam structure. The applicability of these functional parameters to predict ETC is validated in the next section.

6 Comparison and validation

ETC correlations developed in the Sect. 5 for different arrangements and schemes are compared and validated against the experimental and numerical data reported in the literature data for foams of different materials (ceramic and metal).

6.1 With ceramic open-cell foams

Predicted ETC results are firstly compared and validated against the experimental data reported by Dietrich et al. [4] for ceramic foams. Values of δ and δ' of different models are calculated using empirical correlations according to different arrangements and schemes (Models 1, 3, 8, 11 and 12) and further applied them to estimate ETC. The analytical results are presented in Table 2. From Table 2, it can
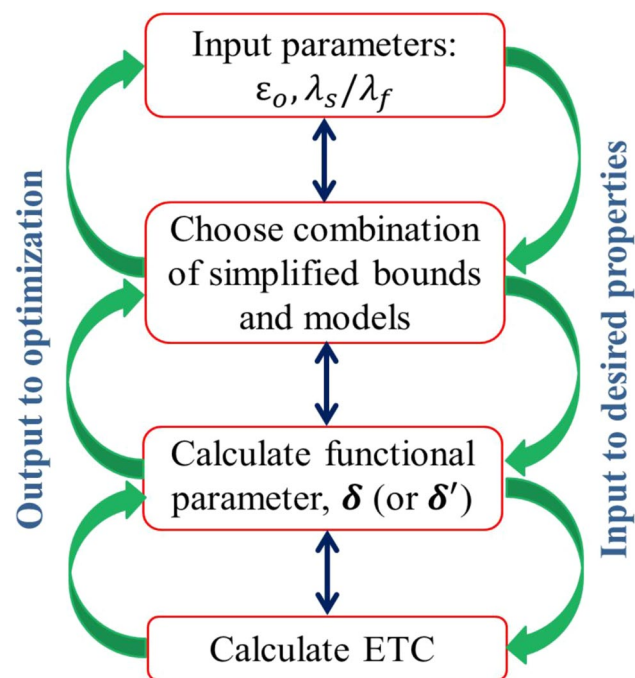
Fig. 5 Algorithm to predict effective thermal conductivity (ETC) by morphological and material properties characteristics of a foam matrix. This algorithm can be used in reciprocal way-from input to output and vice versa

be clearly observed that all these models predict excellent ETC results (see also Fig. 6-left).

6.2 With metal open-cell foams

A few authors (e.g. [9–11]) have already highlighted the problem of non-reporting of intrinsic solid phase conductivity of most of the foams. Most commonly, the correlations that have been reported in the literature were based on parent/bulk solid phase conductivity. Different metal foam materials (or alloys) and their associated ETC values of various authors are presented in Table 3.

Consequently, the methodology described as modified Lemlich model [12] has been used to determine intrinsic solid phase conductivity while using the experimental ETC data. These authors proposed the following formulation of modified Lemlich model that is valid for any arbitrary fluid as:

$$\frac{\lambda_{eff}}{\lambda_f} = \frac{2}{3} \cdot \frac{\lambda_s}{\lambda_f} \cdot (\psi)^{1/F} \tag{30}$$

where,
$F = -0.004\left(ln(\psi^2 \cdot \lambda_s/\lambda_f)\right)^2 + 0.0593 ln(\psi^2 \cdot \lambda_s/\lambda_f) + 0.7144.$

A simple method has been described below to calculate the intrinsic solid phase conductivity (λ_s) for a given ψ, λ_{eff} and λ_f.

Step I: Eq. 30 can be rewritten as:

$$\frac{\lambda_{eff}}{\lambda_f} = \frac{2}{3} \cdot \frac{\lambda_s}{\lambda_f} \cdot (\psi)^{1/\left[-0.004\left(ln(\psi^2 \cdot \lambda_s/\lambda_f)\right)^2 + 0.0593 ln(\psi^2 \cdot \lambda_s/\lambda_f) + 0.7144\right]} \tag{31}$$

Step II: Assign $\lambda_s/\lambda_f = K_s$ and $\lambda_{eff}/\lambda_f = K_e$ and apply natural log functions to both sides:

$$\ln(1.5 \cdot K_e) = ln(K_s)$$
$$+ \frac{1}{\left[n_1\left\{ln\left(\psi^2 \cdot K_s\right)\right\}^2 + n_2\left\{ln\left(\psi^2 \cdot K_s\right)\right\} + n_3\right]} \cdot ln(\psi) \tag{32a}$$

$$\ln(1.5 \cdot K_e) - ln(K_s)$$
$$- \frac{1}{\left[n_1\left\{ln\left(\psi^2 \cdot K_s\right)\right\}^2 + n_2\left\{ln\left(\psi^2 \cdot K_s\right)\right\} + n_3\right]} \cdot ln(\psi) = 0 \tag{32b}$$

where, $n_1 = -0.004$, $n_2 = 0.0593$, $n_3 = 0.7144$.

Step III: Using iterative process, solve for K_s.

Intrinsic solid phase conductivities were calculated using Eqs. 31, 32a for each foam material and these values were subsequently substituted in different models (Models 1, 3, 8, 11 and 12) to predict analytical ETC values (see Table 3). From Table 3, it can be prompted that the different models are consistent with each other

Table 2 Validation of analytically determined effective thermal conductivity (λ_{eff}) of Al_2O_3, Mullite and OBSiC ceramic foams (data taken from Dietrich et al. [4]) of different pore sizes and porosities with air as an interstitial fluid

Material	Experiments			Analytical															
				Model 1			Model 3			Model 8			Model 11			Model 12		
	λ_s	ε_t	λ_{eff}/λ_f	δ_1	λ_{eff}/λ_f	Error (%)	δ_3	λ_{eff}/λ_f	Error (%)	δ'_2	λ_{eff}/λ_f	Error (%)	δ'_5	λ_{eff}/λ_f	Error (%)	δ'_6	λ_{eff}/λ_f	Error (%)
Al_2O_3	26	0.754	*112.39*	0.471	113.49	0.98	0.468	115.36	1.65	0.935	114.60	0.66	0.804	118.26	3.19	0.894	117.05	1.02
		0.808	*89.49*	0.505	83.13	7.11	0.502	84.33	1.44	0.924	84.40	0.08	0.789	87.77	3.99	0.880	86.36	1.61
		0.802	*92.79*	0.501	86.34	6.95	0.498	87.60	1.46	0.925	87.66	0.07	0.791	91.08	3.90	0.882	89.67	1.55
		0.806	*90.01*	0.504	84.19	6.47	0.501	85.42	1.46	0.924	85.48	0.07	0.790	88.87	3.97	0.881	87.46	1.59
		0.809	*93.42*	0.506	82.59	11.59	0.503	83.79	1.45	0.924	83.86	0.08	0.789	87.22	4.01	0.880	85.81	1.62
		0.854	*67.67*	0.534	59.75	11.70	0.531	60.63	1.47	0.910	60.34	0.48	0.771	63.19	4.72	0.863	61.90	2.04
Mullite	4.4	0.736	*22.01*	0.460	21.65	1.64	0.457	23.11	6.74	0.899	21.61	6.49	0.727	22.57	4.44	0.849	22.50	0.31
		0.785	*13.47*	0.491	16.81	24.80	0.488	17.72	5.41	0.886	16.95	4.35	0.709	17.80	5.01	0.834	17.70	0.56
		0.789	*15.48*	0.493	16.43	6.14	0.490	17.32	5.42	0.885	16.58	4.27	0.708	17.42	5.07	0.832	17.32	0.57
		0.793	*18.28*	0.496	16.06	12.14	0.493	16.92	5.35	0.884	16.22	4.14	0.706	17.05	5.12	0.831	16.94	0.65
		0.797	*15.4*	0.498	15.69	1.88	0.495	16.52	5.29	0.882	15.86	4.00	0.704	16.67	5.11	0.829	16.57	0.60
		0.834	*11.94*	0.521	12.40	3.85	0.518	13.02	5.00	0.868	12.60	3.23	0.686	13.29	5.48	0.812	13.20	0.68
OBSiC	15	0.742	*70.43*	0.464	69.93	0.71	0.461	71.74	2.59	0.926	69.88	2.59	0.784	72.26	3.41	0.883	71.82	0.61
		0.791	*52.16*	0.494	53.59	2.74	0.491	54.73	2.13	0.916	53.90	1.52	0.770	56.10	4.08	0.871	55.52	1.03
		0.791	*56.53*	0.494	53.59	5.20	0.491	54.73	2.13	0.916	53.90	1.52	0.770	56.10	4.08	0.871	55.52	1.03
		0.791	*57.09*	0.494	53.59	6.13	0.491	54.73	2.13	0.916	53.90	1.52	0.770	56.10	4.08	0.871	55.52	1.03
		0.786	*48.52*	0.491	55.19	13.75	0.488	56.37	2.14	0.917	55.49	1.56	0.772	57.72	4.02	0.872	57.13	1.02
		0.845	*36.2*	0.528	37.32	3.09	0.525	38.08	2.04	0.900	37.48	1.58	0.749	39.30	4.86	0.850	38.73	1.45

Italics values represent the experimental data while the non-italics values represent the calculated/analytical data
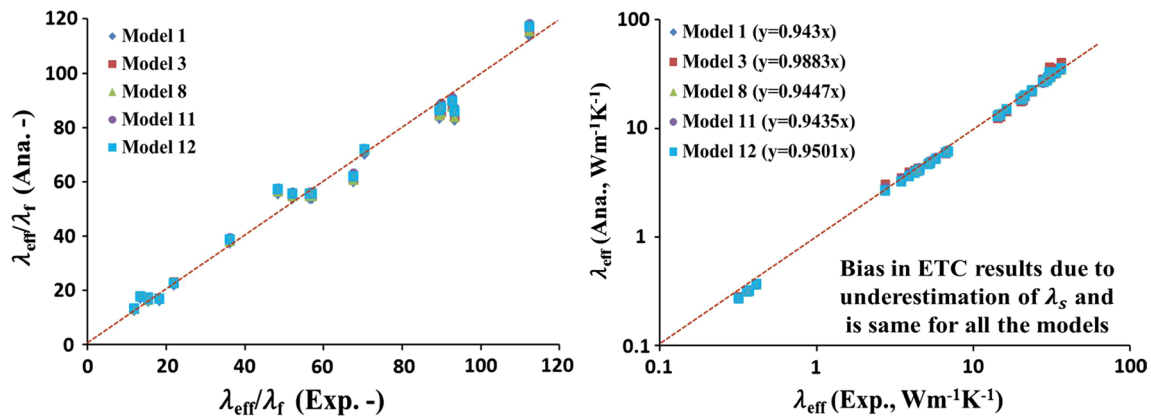
Fig. 6 Comparison and validation of experimentally and analytically obtained effective thermal conductivity (λ_{eff}) data by using different models (Models 1, 3, 8, 11, 12) for ceramic foams (*left*) and metal foams (*right*). Note that, *Ana.* analytical, *Exp.* experimental. The fitting comparison between experimental and analytical ETC values is also presented (*right*). The ETC data of ceramic foams were taken from the works of Dietrich et al. [4] while ETC data of metal foams were taken from Bhattacharya et al. [2], Solórzano et al. [3], Bodla et al. [15], Ranut et al. [19], Wulf et al. [20], Takegoshi et al. [33] and Paek et al. [34]

and their uses can be combined to predict accurate ETC values (see also Fig. 6-right). However, the predicted values underestimate the experimental ETC data which can be attributed to the formulation [12] by which the intrinsic solid phase conductivity of a different material is under-evaluated.

7 Conclusion

Different arrangements of simplified models in arithmetic and geometric schemes were tried and tested to determine effective thermal conductivity of foam samples of different materials. It has been demonstrated that arrangements of different simplified models may work for one scheme but may not work for another.

The highlight of the present work is to significantly improve the notion of fixed value of adjustable parameter and thus, determining a functional parameter of coupled thermal bounds and models as a function of foam material properties and morphology. Their validity and adaptability has been shown to predict accurate ETC values.

The predicted values are compared and validated against experimental data for foams of different materials in a wide porosity range.

It is from this view point, arrangement of Parallel and Series models in both arithmetic and geometric schemes predicts the most accurate effective thermal conductivity results. Moreover, the combination of Parallel and EMT models in the arithmetic scheme as well as Parallel and Reciprocity models, and HS upper bound and Reciprocity models arranged in geometric scheme also predict accurate results.

Depending on the availability of morphological resources, any of these models can be easily used to determine effective thermal conductivity from morphology and thermal conductivity ratio. From the present results, it can be safely concluded that the proposed correlations are most suitable for evaluating the functional parameters of both schemes. Finally, it may be emphasized that the most remarkable feature of the proposed models lies in the fact that they allow one to quite accurately predict the effective thermal conductivity of open-cell foam structures for any working fluid.

Table 3 Determination of intrinsic solid phase conductivity (λ_s) and validation of analytical effective thermal conductivity (λ_{eff}) against experiments for foam samples of different pore sizes and porosities with air as interstitial fluid

Authors	Material	Experiments		Analytical Equations (31, 32)	Model 1			Model 3			Model 8			Model 11			Model 12		
		ε_o	λ_{eff}	λ_s	δ_1	λ_{eff}	Error (%)	δ_3	λ_{eff}	Error (%)	δ'_2	λ_{eff}	Error (%)	δ'_5	λ_{eff}	Error (%)	δ'_6	λ_{eff}	Error (%)
Takegoshi et al. [33]	ERG-Al T6101	0.936	4.4	156.03	0.585	4.17	5.23	0.582	4.20	0.72	0.909	4.11	2.14	0.795	4.21	2.43	0.861	4.01	4.75
		0.908	6.7	147.22	0.567	5.88	12.24	0.564	5.93	0.85	0.926	6.06	2.19	0.813	6.18	1.98	0.882	5.95	3.72
		0.905	6.7	141.70	0.566	5.87	12.39	0.562	5.92	0.85	0.926	6.06	2.36	0.813	6.18	1.98	0.883	5.96	3.56
Paek et al. [34]		0.938	4.25	157.35	0.586	4.06	4.47	0.583	4.09	0.74	0.907	3.98	2.69	0.793	4.09	2.76	0.859	3.89	4.89
		0.92	5.8	152.46	0.575	5.21	10.17	0.572	5.25	0.77	0.920	5.29	0.76	0.807	5.41	2.27	0.875	5.18	4.25
		0.959	2.75	182.24	0.599	3.02	9.82	0.596	3.04	0.66	0.886	2.76	9.21	0.773	2.86	3.62	0.834	2.67	6.64
Bhattacharya et al. [2]		0.905	6.7	141.70	0.566	5.87	12.39	0.562	5.92	0.85	0.926	6.06	2.36	0.813	6.18	1.98	0.883	5.96	3.56
		0.949	3.9	186.32	0.593	3.89	0.26	0.590	3.92	0.77	0.900	3.72	5.10	0.788	3.83	2.96	0.851	3.61	5.74
		0.909	6.7	149.15	0.568	5.89	12.09	0.565	5.93	0.68	0.925	6.06	2.19	0.813	6.19	2.15	0.882	5.95	3.88
		0.906	6.9	147.46	0.566	6.04	12.46	0.563	6.08	0.66	0.927	6.24	2.63	0.814	6.36	1.92	0.884	6.13	3.62
		0.937	4.5	162.34	0.586	4.26	5.33	0.582	4.30	0.94	0.909	4.20	2.33	0.795	4.31	2.62	0.861	4.09	5.10
Solórzano et al. [3]	AlSi7	0.8	14.3	123.74	0.500	12.40	13.29	0.497	12.48	0.65	0.950	13.05	4.57	0.843	13.11	0.46	0.916	12.95	1.22
		0.81	14.9	136.36	0.506	12.82	13.96	0.503	12.90	0.62	0.950	13.55	5.04	0.844	13.63	0.59	0.916	13.43	1.47
		0.81	14.6	133.70	0.506	12.57	13.90	0.503	12.65	0.64	0.950	13.28	4.98	0.843	13.36	0.60	0.915	13.16	1.50
		0.78	20.2	155.89	0.487	17.60	12.87	0.485	17.72	0.68	0.955	18.48	4.29	0.852	18.55	0.38	0.923	18.38	0.92
		0.79	16.4	133.91	0.494	14.26	13.05	0.491	14.36	0.70	0.952	14.99	4.39	0.847	15.05	0.40	0.919	14.89	1.06
		0.78	20.8	160.42	0.487	18.11	12.93	0.485	18.23	0.66	0.955	19.03	4.39	0.852	19.09	0.32	0.923	18.92	0.89
		0.75	20.9	140.06	0.469	18.63	10.86	0.466	18.75	0.64	0.956	19.30	2.93	0.854	19.32	0.10	0.925	19.26	0.31
		0.72	21.4	126.64	0.450	19.53	8.74	0.447	19.67	0.72	0.958	19.95	1.42	0.855	19.93	0.10	0.927	19.97	0.20
		0.72	20	118.47	0.450	18.27	8.65	0.447	18.40	0.71	0.957	18.67	1.47	0.854	18.64	0.16	0.926	18.67	0.16
		0.71	23.6	134.23	0.444	21.68	8.14	0.441	21.84	0.74	0.958	22.05	0.96	0.857	22.01	0.18	0.929	22.10	0.41
		0.7	29.4	160.76	0.437	27.15	7.65	0.435	27.35	0.74	0.960	27.45	0.37	0.861	27.42	0.11	0.931	27.59	0.62
		0.68	28.2	143.84	0.425	26.49	6.06	0.422	26.79	1.13	0.960	26.52	1.01	0.861	26.44	0.30	0.932	26.70	0.98
		0.71	23.9	135.91	0.444	21.95	8.16	0.441	22.11	0.73	0.959	22.32	0.95	0.857	22.29	0.13	0.929	22.37	0.36
		0.65	27.8	128.72	0.406	26.77	3.71	0.404	28.33	5.83	0.960	26.41	6.78	0.861	26.27	0.53	0.933	26.67	1.52
		0.66	31.3	149.40	0.412	29.87	4.57	0.410	30.89	3.41	0.961	29.56	4.31	0.863	29.45	0.37	0.933	29.86	1.39
		0.66	30.1	143.71	0.412	28.73	4.55	0.410	29.72	3.45	0.961	28.45	4.27	0.863	28.34	0.39	0.933	28.73	1.38
		0.63	30.7	146.55	0.394	32.90	7.17	0.391	36.24	10.2	0.961	32.03	11.62	0.865	31.87	0.50	0.935	32.50	1.98
		0.64	33.9	152.05	0.400	32.87	3.04	0.398	35.51	8.03	0.961	32.16	9.43	0.865	32.02	0.44	0.935	32.60	1.81
		0.62	36.5	154.40	0.387	35.96	1.48	0.385	40.31	12.1	0.962	34.78	13.72	0.866	34.60	0.52	0.936	35.37	2.23

Table 3 continued

Authors	Material	Experiments		Analytical	Model 1			Model 3			Model 8			Model 11			Model 12		
		ε_o	λ_{eff}	Equations (31, 32) λ_s	δ_1	λ_{eff}	Error (%)	δ_3	λ_{eff}	Error (%)	δ'_2	λ_{eff}	Error (%)	δ'_5	λ_{eff}	Error (%)	δ'_6	λ_{eff}	Error (%)
Bodla et al. [15]	ERG-Al T6201	0.9131	5.2	124.84	0.571	4.68	10.00	0.567	4.72	0.85	0.919	4.76	0.85	0.804	4.86	2.10	0.875	4.68	3.70
		0.9126	5.21	124.20	0.570	4.69	9.98	0.567	4.73	0.85	0.920	4.77	0.85	0.804	4.86	1.89	0.875	4.69	3.50
		0.9198	4.52	121.11	0.575	4.15	8.19	0.571	4.19	0.96	0.915	4.18	0.24	0.798	4.26	1.91	0.869	4.10	3.76
Ranut et al. [19]	ERG-Al T6101	0.944	3.49	150.13	0.590	3.47	0.57	0.587	3.50	0.86	0.900	3.34	4.57	0.785	3.43	2.69	0.851	3.25	5.25
		0.927	4.57	137.25	0.579	4.24	7.22	0.576	4.27	0.71	0.913	4.23	0.94	0.798	4.33	2.36	0.866	4.15	4.16
		0.929	5.31	162.64	0.581	4.87	8.29	0.577	4.91	0.82	0.915	4.88	0.61	0.802	5.00	2.46	0.869	4.77	4.60
Wulf et al., [20]	FeCrAl-alloy	0.89	0.372	6.09	0.556	0.32	13.98	0.553	0.33	3.13	0.848	0.32	3.03	0.668	0.32	0.00	0.788	0.32	0.00
		0.85	0.415	4.82	0.531	0.36	13.25	0.528	0.37	2.78	0.864	0.36	2.70	0.682	0.36	0.00	0.807	0.37	2.78
		0.87	0.36	4.87	0.544	0.31	13.89	0.541	0.32	3.23	0.853	0.31	3.13	0.670	0.31	0.00	0.795	0.31	0.00
		0.9	0.32	5.76	0.562	0.27	15.63	0.559	0.28	3.70	0.838	0.27	3.57	0.655	0.27	0.00	0.777	0.27	0.00
		0.88	0.37	5.49	0.550	0.32	13.51	0.547	0.33	3.13	0.851	0.32	3.03	0.670	0.32	0.00	0.792	0.32	0.00

Italics values represent the experimental data while the non-italics values represent the calculated/analytical data

References

1. Calmidi VV, Mahajan RL (1999) The effective thermal conductivity of high porosity fibrous metal foams. ASME J Heat Transf 121(2):466–471
2. Bhattacharya A, Calmidi VV, Mahajan RL (2002) Thermophysical properties of high porosity metal foams. Int J Heat Mass Transf 45(5):1017–1031
3. Solorzano E, Reglero JA, Rodriguez-Perez MA, Lehmhus D, Wichmann MA, De Saja JA (2008) An experimental study on the thermal conductivity of aluminium foams by using the transient plane source method. Int J Heat Mass Transf 51:6259–6267
4. Dietrich B, Schell G, Bucharsky EC, Oberacker R, Hoffmann MJ, Schabel W, Kind M, Martin H (2010) Determination of the thermal properties of ceramic sponges. Int J Heat Mass Transf 53(1):198–205
5. Yang XH, Bai JX, Yan HB, Kuang JJ, Lu TJ, Kim T (2014) An analytical unit cell model for the effective thermal conductivity of high porosity open-cell metal foams. Transp Porous Media 102:403–426
6. Wang M, Pan N (2008) Modeling and prediction of the effective thermal conductivity of random open-cell porous foams. Int J Heat Mass Transf 51(5–6):1325–1331
7. Coquard R, Rochais D, Baillis D (2012) Conductive and radiative heat transfer in ceramic and metal foams at fire temperatures. Fire Technol 48:699–732
8. Mendes MAA, Talukdar P, Ray S, Trimis D (2014) Detailed and simplified models for evaluation of effective thermal conductivity of open-cell porous foams at high temperatures in presence of thermal radiation. Int J Heat Mass Transf 68:612–624
9. Miettinen L, Kekalainen P, Turpeinen T, Hyvaluoma J, Merikoski J, Timonen J (2012) Dependence of thermal conductivity on structural parameters in porous samples. AIP Adv 2:012101–012115
10. Kumar P, Topin F, Vicente J (2014) Determination of effective thermal conductivity from geometrical properties: application to open cell foams. Int J Therm Sci 81:13–28
11. Kumar P, Topin F (2014) Simultaneous determination of intrinsic solid phase conductivity and effective thermal conductivity of Kelvin like foams. Appl Therm Eng 71(1):536–547
12. Kumar P, Topin F (2014) The geometric and thermohydraulic characterization of ceramic foams: an analytical approach. Acta Mater 75:273–286
13. Vicente J, Topin F, Daurelle JV, Rigollet F (2006) Thermal conductivity of metallic foam: simulation on real X-ray tomographied porous medium and photothermal experiments. In: Proceedings of IHTC 13, Sydney
14. Coquard R, Baillis D (2009) Numerical investigation of conductive heat transfer in high-porosity foams. Acta Mater 57(18):5466–5479
15. Bodla KK, Murthy JY, Garimella SV (2010) Resistance network-based thermal conductivity model for metal foams. Comput Mater Sci 50:622–632
16. Randrianalisoa J, Coquard R, Baillis D (2013) Microscale direct calculation of solid phase conductivity of Voronoi's foams. J Porous Media 16(5):411–426
17. Mendes AAM, Ray S, Trimis D (2013) A simple and efficient method for the evaluation of effective thermal conductivity

of open-cell foam-like structures. Int J Heat Mass Transf 66:412–422

18. Mendes AAM, Ray S, Trimis D (2014) An improved model for the effective thermal conductivity of open-cell porous foams. Int J Heat Mass Transf 75:224–230

19. Ranut P, Nobile E, Mancini L (2014) High resolution X-ray microtomography-based CFD simulation for the characterization of flow permeability and effective thermal conductivity of aluminum metal foams. Exp Therm Fluid Sci. doi:10.1016/j.expthermflusci.2014.10.018

20. Wulf R, Mendes AAM, Skibina V, Al-Zoubi A, Trimis D, Ray S, Gross U (2014) Experimental and numerical determination of effective thermal conductivity of open cell FeCrAl-alloy metal foams. Int J Therm Sci 86:95–103

21. Krishnan S, Garimella S, Murthy JY (2008) Simulation of thermal transport in open-cell metal foams: effects of periodic unit-cell structure. J Heat Transfer 130(2):24503–24507

22. Druma A, Kharil Alam M, Druma C (2006) Surface area and conductivity of open-cell carbon foams. J Miner Mater Charact Eng 5:73–86

23. Boomsma K, Poulikakos D (2001) On the effective thermal conductivity of a three-dimensionally structured fluid-saturated metal foam. Int J Heat Mass Transf 44:827–836

24. Singh R, Kasana HS (2004) Computational aspects of effective thermal conductivity of highly porous metal foams. Appl Therm Eng 24:1841–1849

25. Leach AG (1993) The thermal conductivity of foams. I: models for heat conduction. J Phys D Appl Phys 26:733–739

26. Hashin Z, Shtrikman S (1962) A variational approach to the theory of the effective magnetic permeability of multiphase materials. J Appl Phys 33:3125–3131

27. Landauer R (1952) The electrical resistance of binary metallic mixtures. J Appl Phys 23(7):779–784

28. Keller JB (1962) A theorem on the conductivity of a composite medium. J Math Phys 5:548–549

29. Pieper M, Klein P (2012) Application of simple, periodic homogenization techniques to non-linear heat conduction problems in non-periodic, porous media. Heat Mass Transf 48:291–300

30. Qu ZG, Wang TS, Tao WQ, Lu TJ (2012) A theoretical octet-truss lattice unit cell model for effective thermal conductivity of consolidated porous materials saturated with fluid. Heat Mass Transf 48:1385–1395

31. Dai Z, Nawaz K, Park Y, Bock J, Jacobi A (2010) Correcting and extending the Boomsma–Poulikakos effective thermal conductivity model for three-dimensional, fluid-saturated metal foams. Int Commun Heat Mass Transf 37(6):575–580

32. del Rio JA, Zimmerman RW, Dawe RA (1998) Formula for the conductivity of a two-component material based on the reciprocity theorem. Solid State Commun 106:183–186

33. Takegoshi E, Hirasawa Y, Matsuo J, Okui K (1992) A study on effective thermal conductivity of porous metals. Trans Jpn Soc Mech Eng B 58:879–884

34. Paek JW, Kang BH, Kim SY, Hyun JM (2000) Effective thermal conductivity and permeability of aluminium foam materials. Int J Thermophys 21(2):453–464